Data-Driven Identification of a Linear Parameter-Varying Model for Overhead Crane Sway Dynamics

Xing-Yi Li*†, Danielle Nyakam Nya†, Franco Falconi *, Tarek Raïssi †
† Conservatoire National des Arts et Métiers (CNAM), EA4629, CEDRIC, Paris, France
* Schneider Electric, Rueil Malmaison, France
Emails: (xingyi.li, danielle.nyakam-nya)@lecnam.net, franco.falconi@se.com, tarek.raissi@cnam.fr

***Abstract*—Overhead cranes are widely used in industrial material handling, where payload oscillation during transport remains a major challenge for safety and positioning accuracy. This paper proposes a data-driven identification framework for linear parameter-varying (LPV) modeling of crane sway dynamics, explicitly accounting for variations in cable length. The approach combines local linear time-invariant (LTI) model identification with a coherence transformation using the state-space Model Interpolation of Local Estimates (SMILE) framework, followed by a global LPV model obtained through a joint optimization balancing time-domain prediction accuracy and local structural consistency. The method is experimentally validated on a laboratory crane under four load conditions using a cross-validation protocol, in which each load condition is successively held out as an unseen test case. This enables a systematic evaluation of the model's generalization capability under realistic industrial variability. Cross-validation results show that joint optimization significantly improves generalization across all load conditions compared to purely interpolated models, while ensuring structurally consistent behavior in low-excitation regimes where purely data-driven approaches typically degrade. The LPV input-output (LPV-IO) model also achieves competitive prediction error across folds, but the state-space formulation provides better robustness and interpretability under varying payloads, making it more suitable for industrial anti-sway applications where payload mass is uncertain.**

***Keywords*–Linear Parameter-Varying system, state-space models, system identification, time-domain validation, subspace methods, SMILE framework, overhead crane**

I. Introduction

Overhead cranes are essential material handling systems widely used across modern industry—from factory workshops and manufacturing lines to warehouses, waste-to-energy plants, and port logistics [1]–[3]. Their basic function is to lift, transport, and position heavy loads within constrained spaces. Their performance directly affects efficiency, safety, and operational reliability. During operation, payload oscillation remains a critical challenge. Large sway reduces positioning accuracy, increases settling time, and may lead to unsafe situations such as collisions or load instability [4], [5]. Therefore, suppressing load swing has become a central issue in both research and industrial applications.

For modeling and control, the payload is often approximated as a point mass suspended by a rigid and massless cable, leading to a single-pendulum model widely adopted for its simplicity and analytical convenience. However, real crane systems deviate from this assumption: the system often includes a hook, spreader, or grab, and the payload usually has a distributed mass [2], introducing additional dynamics that can exhibit double-pendulum or multi-body behavior [6]. Although the double-pendulum model gives a more accurate description, industrial applications typically prioritize robustness and ease of implementation. Higher model complexity introduces more states, nonlinear couplings, and increases the identification effort. As a result, such models are less attractive in practice.

Figure 1 illustrates the considered crane structure: a trolley travels along a bridge girder and carries a suspended load via a cable, with the trolley motion serving as the primary actuation variable [7], [8]. For planar anti-sway modeling, the suspended assembly is represented by a cable and a lumped mass, and the swing angle $\theta(t)$ is the controlled output.

It is worth noting that, under the idealized single-pendulum assumption derived from Lagrangian mechanics, the payload mass cancels in the equations of motion, rendering sway dynamics theoretically independent of the suspended load. However, real crane installations deviate from this ideal in practically relevant ways. The hook and payload assembly form a compound pendulum whose effective suspension length depends on the relative mass distribution between the hook and the load [9]: as payload mass increases, the effective length shifts toward the total cable-plus-hook length, altering the natural frequency in a manner not captured by the ideal model, while load-dependent friction in the drive mechanism introduces additional dissipative effects. These deviations introduce residual load-dependent dynamics that are not captured by the cable length alone. Testing the model under multiple load conditions, therefore, provides a meaningful and challenging assessment of its robustness to unmodeled physical effects.

In many industrial settings, the rope length is more appropriately treated as a measurable scheduling parameter rather than as a control input, given the structural constraints of the hoisting mechanism and its role as a safety-critical component subject to wear and fatigue. Gain-scheduled and LPV control strategies have been explored for overhead cranes [10]–[12], typically relying on analytically derived models. Classical physics-based models often fail to capture these effects accurately under varying operating conditions, especially when

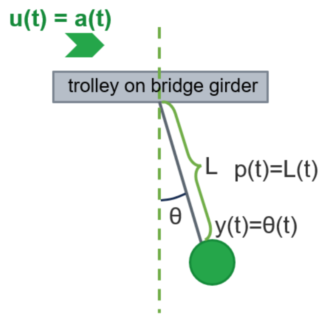

(a) Real overhead crane (unloaded case)

(b) Simplified model (single-pendulum)

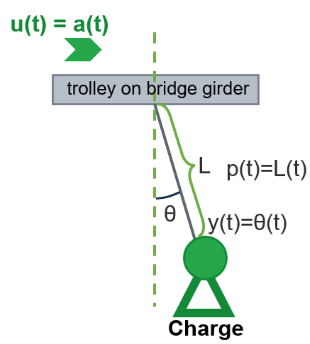

(c) Real overhead crane (loaded case)

(d) Model with payload (lumped mass)

Fig. 1: Overhead crane structure: real system views and corresponding simplified planar models. The trolley motion provides the excitation, the sway angle is $\theta(t)$, and the cable length $L(t)$ serves as the LPV scheduling variable.

unmodeled dynamics and measurement noise are present. Obtaining accurate LPV models directly from experimental data remains challenging, especially when both load and scheduling conditions vary simultaneously. In particular, independently identified local models may not share a consistent state basis, which prevents direct interpolation and motivates the use of coherence transformation techniques such as SMILE.

The present work builds upon the combined global-local optimization framework of [13] and provides several contributions from both methodological and experimental perspectives. First, the framework is validated on an experimental overhead crane under simultaneous variations of cable length and payload mass across four load conditions (0, 20, 40, and 60 kg), enabling a systematic assessment of robustness in the presence of unmodeled physical effects. Second, a cross-validation protocol is adopted, where each load condition is alternately excluded from training and used for validation. This provides a more systematic evaluation of model generalization under varying operating conditions. Such a setting provides a realistic and challenging evaluation of interpolation capability under conditions representative of industrial deployment. Third, the behavior of the identified models is specifically analyzed in low-excitation regimes, corresponding to stationary trolley phases where the input signal carries limited information. This analysis highlights significant differences in structural robustness between the approach and purely data-driven alternatives. Finally, a systematic four-way comparison between the Global+Local LPV state-space model, a least-squares LPV-IO model, and two interpolated baseline models provides quantitative insight into the trade-off between prediction accuracy and structural interpretability, which is critical for subsequent LPV control design.

The remainder of this paper is organized as follows. Section II introduces the LPV identification framework, covering persistent excitation conditions, the local LTI identification procedure, the SMILE coherence transformation, and global LPV model construction with joint optimization. Section III presents experimental validation on a laboratory crane testbed, comparing the LPV state-space, LPV-IO, and interpolated local models under various load conditions. Section IV concludes and outlines directions for future work.

II. LPV Identification Framework for Overhead Crane Systems

The identification methods in the LPV field are typically classified as either LPV-IO or LPV state-space (LPV-SS) approaches. This section presents the framework adopted in this work for a second-order discrete-time LPV model. The method follows a local-to-global strategy: starting from constant-scheduling data segments, local LTI models are identified, transformed into a coherent state-space basis using the SMILE framework, and then combined to construct a global LPV model jointly fitted to the coherent local models and the global time-domain data.

A. Persistent Excitation and Data Requirements

In LPV identification, data richness is essential for parameter uniqueness, consistency, and trajectory reconstruction. For the local LTI models (frozen models at fixed p), classical persistent excitation (PE) remains critical: the input must be sufficiently rich to reliably identify each local subsystem. However, extending PE from LTI to LPV systems is nontrivial. In LPV systems, regressors depend on both signal dynamics and scheduling-dependent basis functions. As a result, the concept of “PE of order n” is not well-defined in the LPV context [14]. Instead, the focus shifts to data informativity, i.e., whether the dataset is sufficiently rich for a given parametrization and model order [14].

This viewpoint was formalized in the prediction-error framework, where identifiability depends jointly on model structure and data [15]. For LPV-IO or quasi-LPV models, two conditions are required [16], [17]:

- the scheduling variable must explore sufficiently many operating points;
- the input must excite the corresponding local LTI models.

Thus, PE is no longer a property of the input alone, but of the combined input–scheduling data.

More recent work reformulates this concept as generalized persistent excitation (LPV-GPE). In this framework, data richness is defined by a rank condition on a joint Hankel matrix constructed from the input, output, and scheduling signals. If this matrix is of full rank, the data can span all admissible trajectories and enable finite-horizon reconstruction [18]. This principle underlies modern data-driven control methods, such as LPV-DeePC [19]. In practice, both the input excitation and the scheduling variation must be sufficiently rich to ensure reliable identification of the local models.

B. System Description

A single-input single-output (SISO) overhead crane system with a load suspended by a cable of variable length is considered. The input is the trolley acceleration $u(t) = a(t)$, the output is the swing angle $y(t) = \theta(t)$, and the scheduling variable is the cable length $p(t) = L(t)$. Under the small-angle assumption ($|\theta| \ll 1$), the crane dynamics can be approximated as linear in the signals, while its coefficients depend on the scheduling variable $L(t)$. Consequently, the system naturally fits within the LPV framework.

C. Discrete-Time LPV Model for the Overhead Crane

An LPV system is a dynamic system that is linear in its signals but whose coefficients depend on a measurable scheduling variable $L(t)$. When $L(t) = L^\star$ is constant, the system reduces to a local frozen LTI model.

1) Input-Output Representation: In Discrete-Time (DT) system, using a sampling period T_s, the discrete-time representation takes the form:

$$y(k) = \sum_i a_i(L(k), L(k-1), \dots)y(k-i) + \sum_j b_j(L(k))u(k-j) \tag{1}$$

where the dependence on L may become dynamic due to discretization.

2) State-Space Representation: For a fixed parameter $L(t) = L^\star$, the model reduces to a standard LTI state-space form; for varying $L(k)$, the matrices become scheduling-dependent:

$$x_{k+1} \approx A(L_k, L_{k-1})x_k + B(L_k)u_k \tag{2}$$

This introduces dynamic dependence on the scheduling variable.

D. Local vs Global Identification

1) Local Identification: Local identification consists of applying a classical identification procedure at different operating points of the system, defined by constant trajectories of the scheduling variables, and allows the determination of local LTI models that may have different structures [14]. At each operating point L_i, the system is excited with $u(t)$, and a local LTI model A_i, B_i, C_i, D_i is identified via subspace methods. The resulting set of local models is then used as the basis for the SMILE coherence step. The local models are not directly comparable because they may have different state bases.

To solve this, the SMILE (State-space Model Interpolation of Local Estimates) method is used. SMILE seeks transformation matrices T_{L_i} such that:

$$H_\ell = \begin{bmatrix} A_{L_i} & B_{L_i} \\ C_{L_i} & D_{L_i} \end{bmatrix} = \begin{bmatrix} T_{L_i}\tilde{A}_{L_i}T_{L_i}^{-1} & T_{L_i}\tilde{B}_{L_i} \\ \tilde{C}_{L_i}T_{L_i}^{-1} & \tilde{D}_{L_i} \end{bmatrix} \tag{3}$$

After this step, all matrices $\{A_{L_i}, B_{L_i}, C_{L_i}, D_{L_i}\}$ become comparable.

Following [20], the observability-based construction is adopted here as an illustrative example. Since the local models are second order $n_x = 2$, for the SISO case, each local model, the observability matrix $\tilde{O}_i$is defined as follows.

$$\tilde{O}_i = \begin{bmatrix} \tilde{c}_1^{(i)} & \tilde{c}_2^{(i)} \\ \tilde{c}_1^{(i)}\tilde{a}_{11}^{(i)} + \tilde{c}_2^{(i)}\tilde{a}_{21}^{(i)} & \tilde{c}_1^{(i)}\tilde{a}_{12}^{(i)} + \tilde{c}_2^{(i)}\tilde{a}_{22}^{(i)} \end{bmatrix}. \tag{4}$$

The reason this matrix is useful is that it transforms in a clean way under a state change. From (3), one obtains

$$\tilde{O}_i = O_S(L_i)\tilde{T}_i^{-1}, \tag{5}$$

where

$$O_S(L_i) = \begin{bmatrix} C_S(L_i) \\ C_S(L_i)A_S(L_i) \end{bmatrix} \tag{6}$$

is the observability matrix of the static part of the system at scheduling value L_i. The SMILE transformation is defined as

$$T_i = \tilde{O}_1^\dagger \tilde{O}_i, \tag{7}$$

where $\tilde{O}_1^\dagger$ is the Moore–Penrose pseudoinverse of the observability matrix of the reference model. Geometrically, T_i maps the state coordinates of the i-th local model onto those of the reference model, so that after transformation, all local A_i, B_i, C_i matrices live in the same coordinate frame and can be meaningfully interpolated as functions of L. Without this step, the variation of local matrices with respect to L would reflect coordinate inconsistencies rather than true physical dependencies.

Substituting (5) into (7) gives

$$T_i = \tilde{O}_1^\dagger O_S(L_i)\tilde{T}_i^{-1}. \tag{8}$$

This shows that $T_i\tilde{T}_i$ is not arbitrary and why the transformed local models become coherent.

Once T_i is computed, the local matrices are transformed according to (3). The transformed input matrix is

$$B_i = T_i\tilde{B}_i = \begin{bmatrix} t_{11}^{(i)} & t_{12}^{(i)} \\ t_{21}^{(i)} & t_{22}^{(i)} \end{bmatrix} \begin{bmatrix} \tilde{b}_1^{(i)} \\ \tilde{b}_2^{(i)} \end{bmatrix} = \begin{bmatrix} t_{11}^{(i)}\tilde{b}_1^{(i)} + t_{12}^{(i)}\tilde{b}_2^{(i)} \\ t_{21}^{(i)}\tilde{b}_1^{(i)} + t_{22}^{(i)}\tilde{b}_2^{(i)} \end{bmatrix}. \tag{9}$$

The transformed output matrix is $C_i = \tilde{C}_iT_i^{-1}$and the transformed state matrix is $A_i = T_i\tilde{A}_iT_i^{-1}$. This left-right multiplication is necessary because A_i maps state to state. The left multiplication changes the coordinates of the next state. The right multiplication changes the coordinates of the current state.

For a second-order SISO local model, the SMILE using the controllability matrix $\tilde{\mathcal{C}}_i = \begin{bmatrix} \tilde{B}_i & \tilde{A}_i\tilde{B}_i \end{bmatrix}$ may then define

$$T_i = \tilde{\mathcal{C}}_1 \tilde{\mathcal{C}}_i^{\dagger}. \tag{10}$$

In practice, one may test both the observability route and the controllability route, check condition numbers, and keep the version that produces smoother coherent matrices.

2) Global Identification: After obtaining coherent local models, global identification estimates a single LPV model over the whole domain as: $A(L) = A_0 + \psi_1(L)A_1 + \psi_2(L)A_2$, where $A_i \in \mathbb{R}^{2\times 2}$.

Because the same basis functions are used for each matrix, the parameterization stays compact and the model remains easy to interpret.

Fitting only local matrices may degrade time-domain accuracy, whereas fitting only global data may distort the coherent local structure. As in [13], global and local information can be combined in one optimization problem. For a sequence of measured data, define the model output $\hat{y}_k$ obtained by simulating

$$e_k = y_k - \hat{y}_k. \tag{11}$$

The global time-domain cost is

$$J_{\text{global}} = \sum_{k=1}^{N} e_k^2, \tag{12}$$

where N is the number of samples used in the global fit. At each local operating point L_i, the global parameterization predicts $A(L_i), B(L_i), C(L_i), D(L_i)$. These should match the coherent local matrices A_i, B_i, C_i, D_i.

Therefore define

$$J_{\text{local}} = \sum_{i=1}^{m} \sum_{M\in\{A,B,C,D\}} \|M(L_i) - M_i\|_F^2 \tag{13}$$

where $\|\cdot\|_F$ is the Frobenius norm.

This term ensures that the global LPV model remains close to the coherent local models obtained from fixed-L identification. The final objective is

$$J = \alpha J_{\text{global}} + \beta J_{\text{local}}, \tag{14}$$

with $\alpha \geq 0, \beta \geq 0,$ and $\alpha + \beta = 1$. α controls the importance of global time-domain accuracy, β controls the importance of local matrix consistency.

This formulation reflects a trade-off between prediction accuracy and structural consistency: the global term ensures time-domain performance, while the local term preserves the coherence of the identified LPV structure.

III. Experimental Results

The above framework is validated on a laboratory overhead crane to assess its ability to generalize across load conditions not seen during training and to maintain structural consistency under varying excitation levels. Measured data were collected from onboard sensors: the input is the trolley acceleration $u(t) = a(t)$ (numerically derived from velocity), the output is the swing angle $y(t) = \theta(t)$, and the cable length $p(t) = L(t)$ serves as the scheduling variable. Data were sampled at $T_s = 0.5$ s. Experiments covered four load conditions: 0 kg (4 338 samples), 20 kg (5 768 samples), 40 kg (8 016 samples), and 60 kg (6 520 samples). A cross-validation protocol is adopted: in each set, one load condition is entirely withheld from training and used as the held-out test case, while the remaining three conditions constitute the training set. Within each set, the system was recorded at different trolley positions and cable lengths, reflecting realistic intermittent variations. Detailed results are shown for one representative validation case. Training and validation inputs are shown in Figs. 2 and 3. Before identification, signals were preprocessed: spectral analysis identified noise components, followed by filtering to improve data quality. Segments with approximately constant cable length were extracted from both training and validation sets. Persistent excitation analysis was performed on training segments, and those meeting the PE condition were used to identify local LTI state-space models via subspace methods. Segments with insufficient input variation (e.g., short idle intervals) were discarded. In total, 32 groups of constant-length segments were obtained from the training set, with corresponding segments in the validation set. These local models capture system dynamics for cable lengths from approximately 0.6 m to 1.2 m, illustrated as blue curves in Fig. 4.

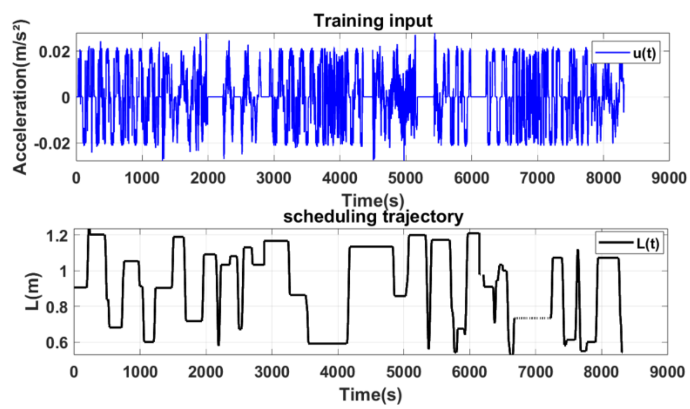

Fig. 2: Training input

Next, the SMILE framework is applied to obtain a set of consistent local models, ensuring agreement across different operating conditions. Both observability- and controllability-based transformations are tested. As shown in Fig. 4, before the SMILE transformation (Raw), the A_{21} and B_1 entries exhibit large scatter, reflecting the basis ambiguity of independently estimated state-space models. After the observability-based transformation (Obs), the entries vary smoothly and monotonically with L, consistent with the $1/L$ dependence predicted by the Lagrangian model. This confirms that the identified LPV structure captures the underlying physical relationship. The controllability-based transformation (Ctrb) yields

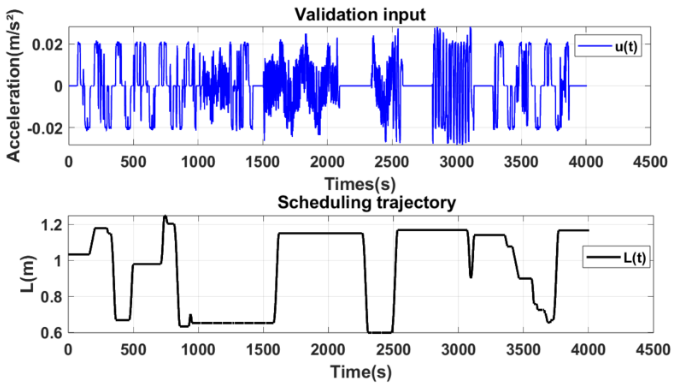

Fig. 3: Validation input

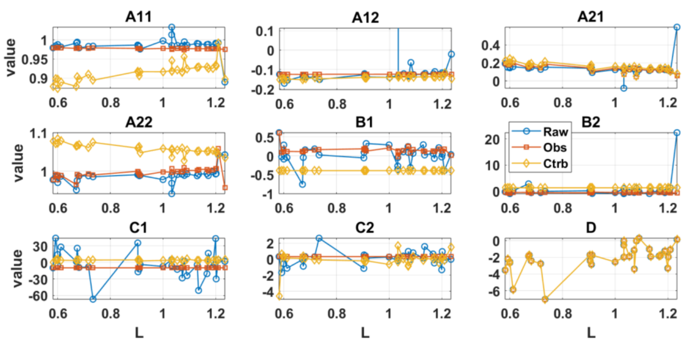

Fig. 4: Values of the 32 sets of LTI model matrices arranged in L-order after SMILE

similar results but with slightly higher condition numbers; thus, the observability route is retained.

Two global LPV models are then constructed. The first is an affine LPV model using the basis function $f_{b1}(L) = x_0 + x_1 L(t)$, and the second is a quadratic LPV model using $f_{b2}(L) = x_0 + x_1 L(t) + x_2 L(t)^2$. These models parameterize the system matrices as functions of the cable length.

Output reconstruction is evaluated on the validation dataset. The difference between reconstructed and measured outputs is shown in Fig. 6 with purple and red dashed lines. The quadratic model achieves lower reconstruction error than the affine model, indicating that crane dynamics depend nonlinearly on L. Higher-order parametrizations were not considered to avoid overfitting and preserve interpretability. Therefore, the quadratic pattern is retained for the subsequent global stage.

A key aspect of the method in [13] is the combined optimization strategy. Fitting the global model solely to local state-space matrices preserves local structure but may degrade time-domain accuracy. Conversely, fitting only to minimize global prediction error can improve simulation performance but distort the structure learned from local models.

To address this trade-off, both global time-domain accuracy and local model consistency are incorporated into a unified objective function. The global model follows the parameterization in Eq. (15). A parameter sweep with a step of 0.05 is performed to study the influence of the weighting between global and local objectives. Results show that as long as

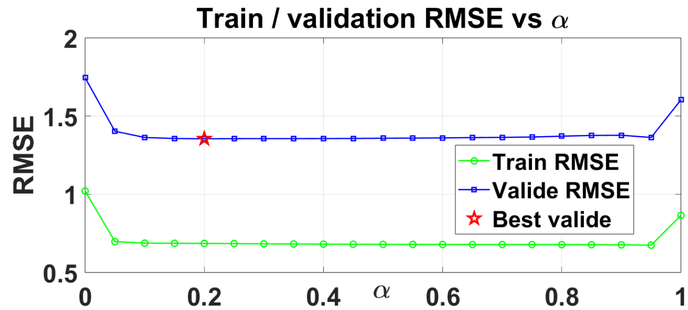

Fig. 5: The RMSE of the outputs reconstructed using the training and validation datasets, compared to the original records, under different values of α

the weight difference is less than one order of magnitude, performance remains largely unchanged (refer to Fig. 5). This indicates that the proposed method is robust to the choice of weighting parameters, which is desirable for practical implementation. In Fig. 6, the blue solid line corresponds to the best RMSE, obtained with $\alpha = 0.2$.

$$M(L) = M_0 + LM_1 + \frac{1}{L^2}M_2, \quad M \in \{A, B, C, D\} \tag{15}$$

In addition, a second-order LPV-IO model (see Equation 1) is identified using a least-squares method. The basis functions are defined as $a_i(L) = a_{i0} + a_{i1}L + a_{i2}\frac{1}{L^2}$, $b_i(L) = b_{i0} + b_{i1}L + b_{i2}\frac{1}{L^2}$. The reconstruction error of this model on the validation set is shown in Fig. 6 using a green dashed line.

Higher-order LPV-IO and LPV state-space models were also tested. However, the second-order models provided the best trade-off between accuracy and robustness. Higher-order models increased the risk of divergence and introduced additional parameters, which would complicate the subsequent control design.

Table I summarizes the cross-validation results across all four sets. The Global+Local model is the only approach that achieves positive fit percentages across all load conditions, confirming consistent generalization throughout the tested range. The LPV-IO model performs competitively on the 20 kg and 60 kg sets, but produces a negative fit percentage on the 0 kg set. The affine and quadratic models fail on several sets and even diverge at 60 kg. This indicates that interpolation alone cannot capture the system dynamics under simultaneous variations of cable length and load.

The LPV-IO model's low RMSE is due to its direct least-squares fit to the global time-domain data. However, this purely data-driven approach does not enforce consistent parameter variation across operating points, limiting interpretability and control applicability. The Global+Local state-space model has slightly higher prediction error but ensures coherent parameter variation with respect to the scheduling variable. It also performs better during low-excitation intervals (approximately 2200–2400 s, 2600–2800 s, and the last 150 s of the validation set; refer to Figs. 3 and 6), where limited input information typically degrades identifiability and increases noise sensitivity. In these regimes, incorporating local model structure helps maintain consistent behavior and prevents unrealistic responses.

The limited performance of purely interpolated affine and quadratic models further highlights the need for the joint optimization strategy: without global time-domain information, interpolation alone is insufficient to capture the system dynamics. These observations confirm that combining local structural information with global prediction-error minimization provides a balanced trade-off between accuracy and structural consistency.

TABLE I: Cross-validation results across four load conditions

Charge	Model	Validation fit (%)	Validation RMSE
0	Global+Local	0.83	1.536
	LPV-IO	-8.98	1.679
	Affine	-38.92	2.119
	Quadratic	-109.04	3.16
20	Global+Local	55.08	0.5077
	LPV-IO	21.21	0.8136
	Affine	8.43	0.9329
	Quadratic	-1033.97	11.1
40	Global+Local	32.061	1.443
	LPV-IO	42.673	1.248
	Affine	-60.802	3.243
	Quadratic	-10.032	2.248
60	Global+Local	30.93	0.9852
	LPV-IO	33.35	0.9559
	Affine	Divergent	1.556e+28
	Quadratic	Divergent	1.391e+30

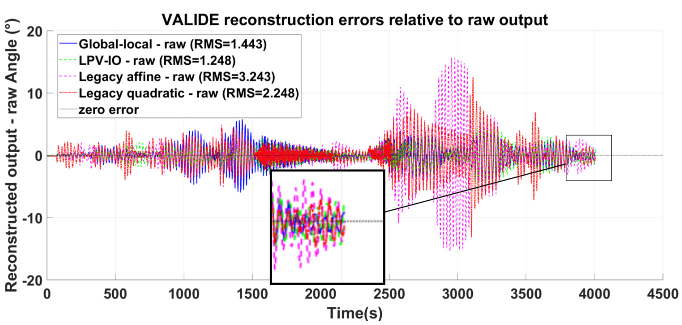

Fig. 6: Error of validation outputs

IV. Conclusion

This paper presented a data-driven LPV identification framework for an overhead crane, with cable length as the scheduling variable governing swing dynamics. Local LTI models identified at constant cable-length operating points were aligned into a common basis using the SMILE coherence transformation. A global LPV model was then estimated by jointly minimizing time-domain prediction error and local matrix consistency, with the trade-off controlled by the weighting parameter α.

Experimental validation using a cross-validation protocol across four load conditions (0, 20, 40, and 60 kg) shows that the Global+Local model is the only approach that achieves positive fit percentages on all sets. Purely interpolated baseline models fail to generalize under simultaneous variations of load and scheduling and exhibit divergence at boundary conditions such as 60 kg. This confirms that global time-domain information is necessary for reliable generalization. The LPV-IO model achieves competitive RMSE on individual sets, but its performance is less consistent near the boundaries of the operating range.

These findings indicate that the framework provides a practical bridge between data-driven identification and control-oriented LPV modeling. Future work includes integrating the LPV model into a gain-scheduled or LPV controller to assess anti-sway performance, analyzing the sensitivity of the SMILE transformation to noise and model-order mismatch, and applying the framework to larger industrial cranes with non-negligible rope dynamics to evaluate broader applicability.

References

[1] E. M. Abdel-Rahman, A. H. Nayfeh, and Z. N. Masoud, "Dynamics and control of cranes: A review," Journal of Vibration and Control, vol. 9, no. 7, pp. 863–908, 2003.

[2] A. Benhidjeb et al., "Modeling and control of overhead cranes: A review," Control Engineering Practice, vol. 21, pp. 1123–1135, 2013.

[3] N. Sun, Y. Fang, and X. Zhang, "Energy-efficient control of port cranes," Energy, vol. 122, pp. 1–13, 2017.

[4] W. J. O'Connor, "A gantry crane problem solved," Journal of Dynamic Systems, Measurement, and Control, vol. 119, no. 2, pp. 233–237, 1997.

[5] W. Singhose, L. Porter, T. Tuttle, and N. Singer, "Vibration reduction using multi-hump input shapers," Journal of Dynamic Systems, Measurement, and Control, vol. 122, no. 3, pp. 443–447, 2000.

[6] L. Ramli, Z. Mohamed, and A. M. Abdullahi, "Control strategies for crane systems: A comprehensive review," Mechanical Systems and Signal Processing, vol. 95, pp. 1–23, 2017.

[7] ASME, "ASME B30.2-2016: Overhead and gantry cranes," 2016, industry standard terminology and definitions.

[8] American Crane & Equipment Corporation, "Crane terminology," 2024, industry glossary defining bridge, bridge girder, trolley, and related overhead-crane terms.

[9] M. R. Mojallizadeh, B. Brogliato, and C. Prieur, "Modeling and control of overhead cranes: A tutorial overview and perspectives," Annual Reviews in Control, vol. 56, p. 100877, 2023.

[10] G. Corriga, A. Giua, and G. Usai, "An implicit gain-scheduling controller for cranes," IEEE Transactions on Control Systems Technology, vol. 6, no. 1, pp. 15–20, 1998.

[11] K. Zavari, G. Pipeleers, and J. Swevers, "Gain-scheduled controller design: Illustration on an overhead crane," IEEE Transactions on Industrial Electronics, vol. 61, no. 7, pp. 3713–3718, 2014.

[12] M. Ermidoro, A. L. Cologni, S. Formentin, and F. Previdi, "Fixed-order gain-scheduling anti-sway control of overhead bridge cranes," Mechatronics, vol. 39, pp. 237–247, 2016.

[13] D. Turk, G. Pipeleers, and J. Swevers, "A combined global and local identification approach for lpv systems," in IFAC-PapersOnLine, vol. 48, no. 28, 2015, pp. 184–189.

[14] R. Tóth, Modeling and Identification of Linear Parameter-Varying Systems. Springer, 2010.

[15] R. Tóth, P. S. C. Heuberger, and P. M. J. V. den Hof, "Prediction-error identification of lpv systems: Present and beyond," in Control of Linear Parameter Varying Systems with Applications. Springer, 2012, pp. 27–60.

[16] X. Wei and L. D. Re, "On persistent excitation for parameter estimation of quasi-lpv systems and its application in modeling of diesel engine torque," in Proceedings of the 14th IFAC Symposium on System Identification, 2006, pp. 517–522.

[17] X. Wei, "Advanced lpv techniques for diesel engines," Ph.D. dissertation, Johannes Kepler University Linz, 2006.

[18] C. Verhoek, I. Markovsky, S. Haesaert, and R. Tóth, "A behavioral approach for lpv data-driven representations," IEEE Transactions on Automatic Control, 2025, also available as arXiv:2412.18543.

[19] T. B. Hamdan, P. Coirault, G. Mercère, and T. Dairay, "Data-enabled predictive control of lpv systems," Control Engineering Practice, 2024.

[20] J. de Caigny, R. Pintelon, J. Camino, and J. Swevers, "Interpolated modeling of lpv systems based on observability and controllability," in IFAC Symposium on System Identification, 2013, pp. 1773–1778.